Reactivity of the CF_3CFHO Radical: Thermal Decomposition and Reaction with O_2†

Fuxiang Wu and Robert W. Carr*

Department of Chemical Engineering and Materials Science, University of Minnesota, 421 Washington Avenue S.E., Minneapolis, Minnesota 55455

Received: April 30, 2003; In Final Form: September 2, 2003

The kinetics of CF_3CFHO radical reactions was studied at 20 and 35 Torr and from 259 to 297 K by flash photolysis with time-resolved mass spectrometry. The CF_3CFHO_2 radical was generated by flash photolysis of Cl_2 in the presence of CF_3CFH_2 and O_2, and CF_3CFHO was formed by the reaction of CF_3CFHO_2 with Cl and by the peroxy radical self-reaction. The rate coefficient ratio for (1) $CF_3CFHO + O_2 \rightarrow CF_3C(O)F + HO_2$ and (2) $CF_3CFHO \rightarrow HC(O)F + CF_3$ was determined by observing the formation of HC(O)F as a function of the partial pressure of O_2. At 20 Torr, $k_1/k_2 = (2.4 \pm 0.8) \times 10^{-25}\ e^{(4248\pm550)/T}\ cm^3\ molecule^{-1}$, and at 35 Torr, $k_1/k_2 = (9.1 \pm 3.3) \times 10^{-26}\ e^{(4370\pm500)/T}\ cm^3\ molecule^{-1}$. Ab initio molecular orbital calculations for optimized geometries, vibrational frequencies, and total energies of CF_3CFHO, the reaction products, and the C−C bond-breaking transition state were made. Energies were calculated by the G2 and G2(MP2) methods. An RRKM model for reaction 2 was based on geometries and energies from the ab initio calculations. RRKM calculated values of k_2 were combined with the experimentally determined k_1/k_2 to estimate k_1. Comparisons were made with estimates made with two other RRKM models (Schneider, W. F.; Wallington, T. J.; Barker, J. R.; Stahlberg, E. A. *Ber. Bunsen-Ges. Phys. Chem.* **1998**, *102*, 1850; Somnitz, H.; Zellner, R. *Phys. Chem. Chem. Phys.* **2001**, *3*, 2352). The ab initio calculations predict the 298 K enthalpy of formation of CF_3CFHO to be −203.0 kcal mol^{-1} (G2MP2) and −203.4 kcal mol^{-1} (G2).

Introduction

Halogenated alkoxy radicals are intermediates in the oxidative degradation of halogenated hydrocarbons in the atmosphere, but there is relatively little quantitative information on their reaction rates and products, compared with that of many other trace species of importance in the atmosphere. The work reported here on reactions of CF_3CFHO radicals is part of an effort to understand the chemical reactivity of halogenated alkoxy radicals better. The CF_3CFHO radical is an intermediate in the atmospheric oxidation of CF_3CFH_2 (HFC-134a), which is a replacement for CF_2Cl_2 (CFC-12) in refrigeration and air conditioning. It is well known that at pressures and temperatures characteristic of the troposphere CF_3CFHO reacts with O_2 and undergoes unimolecular C−C bond scission, reactions 1 and 2.[1−12]

$$CF_3CFHO + O_2 \rightarrow CF_3C(O)F + HO_2 \quad (1)$$

$$CF_3CFHO \rightarrow CF_3 + HC(O)F \quad (2)$$

The rate coefficient ratio, k_1/k_2, has been experimentally determined several times at total pressures in the vicinity of 1−2 atm.[1−7] Wallington and Kaiser[12] have corrected the pressure-dependent k_1/k_2 (reaction 2 is in the unimolecular falloff) from refs 1−7 to the common pressure of 760 Torr and have recommended eq 3 to express the temperature dependence of k_1/k_2 at 760 Torr.

$$\left[\frac{k_1(T)}{k_2(T)}\right]_{760\ \mathrm{Torr}} = (2.4^{+1.6}_{-1.0}) \times 10^{-25} e^{(3590\pm150)/T}\ cm^3\ molecule^{-1} \quad (3)$$

In all of the work summarized by eq 3, reaction 4 was an important source of CF_3CFHO radicals. The data were all taken from experiments in which NO was excluded, thus avoiding the formation and decomposition of chemically activated CF_3CFHO formed by the reaction of NO with CF_3CFHO_2.[7]

$$2CF_3CFHO_2 \rightarrow 2CF_3CFHO + O_2 \quad (4)$$

In the atmosphere, $CF_3C(O)F$ formed by reaction 1 can hydrolyze to $CF_3C(O)OH$, a plant phytogen, and it is necessary to know k_1/k_2 to evaluate the fraction of CF_3CFHO that is converted to $CF_3C(O)OH$. Because of the pressure dependence of k_1/k_2, it is important to determine this ratio at pressures lower than 760 Torr and also at temperatures below 298 K to assess $CF_3C(O)F$ formation throughout the troposphere and stratosphere. The pressure dependence of k_1/k_2 has been reported at 297 K,[1] 295 K,[7] and 269 K.[7] A value of k_1/k_2 is also available at 295 K and 50 mbar.[5]

We report here an experimental determination of the temperature dependence of k_1/k_2 from 259 to 297 K at 35 Torr and at 20 Torr. We also report ab initio molecular orbital molecular structure and energy calculations and an RRKM model for k_2 that is based on the ab initio calculations. Schneider et al.[10] and Somnitz and Zellner[11] have also developed RRKM models of k_2 based on quantum chemical calculations. The former

† Part of the special issue "Charles S. Parmenter Festschrift".

* To whom correspondence should be addressed. E-mail: carrx002@umn.edu.

10.1021/jp030566k CCC: $25.00
Published on Web 11/13/2003

RRKM model gives the high-pressure rate coefficient of eq 5,

$$k_{2\infty} = 4.8 \times 10^{13} \exp(-5737/T)\ \mathrm{s}^{-1} \quad (5)$$

and the latter RRKM model gives the high-pressure rate coefficient of eq 6.

$$k_{2\infty} = 3.8 \times 10^{13} \exp(-6414/T)\ \mathrm{s}^{-1} \quad (6)$$

RRKM models provide a means for scaling k_1/k_2 to other pressures and temperatures. In combination with k_1/k_2, RRKM models for k_2 also permit estimates of the absolute value of k_1 to be made. The only experimental determinations of absolute values for k_1 and k_2 are an Arrhenius expression for k_2 at 230 Torr[8] and a determination of k_1 and k_2 at 295 K and 50 mbar.[5] Estimates of k_1 made from experimental determinations of k_1/k_2 and RRKM models of k_2 are made and discussed.

Experimental Section

Detailed descriptions of the experimental techniques and procedures have been published previously.[14−16] A brief description is given here. The electron ionization quadrupole mass spectrometer was interfaced with a temperature-controlled photolysis reactor by a 50-μm pinhole. A 1-μs Xenon flash lamp was repetitively pulsed at 5 Hz. The reactor was continuously purged by the flow of the reaction mixture at a sufficient rate (about 7 cm/s) to completely sweep away the reaction products between flashes. Electron ionization energies of 15 to 30 eV were employed to reduce fragmentation. Current pulses from a Daly detector were preamplified, discriminated, and signal-averaged with a multichannel analyzer. The number of flashes per experiment was usually 6000, but in some cases up to 9000 flashes were used. Because of the influence of the molecular velocity distribution,[17] data recorded before 0.2 ms was excluded from processing. Also, the sweep of the purge flow imposed an additional decay rate on data acquired after 30 ms. The experiments were designed to avoid interference by these factors.

The CF_3CFHO radical was generated by flash photolysis of Cl_2 in the presence of CF_3CFH_2 and O_2. Reactions 8, 9, 10, and 4 constitute the most important reactions by which CF_3CFHO is generated.

$$Cl_2 + h\nu \rightarrow 2Cl \quad (7)$$

$$CF_3CFH_2 + Cl \rightarrow CF_3CFH + HCl \quad (8)$$

$$CF_3CFH + O_2 \rightarrow CF_3CFHO_2 \quad (9)$$

$$CF_3CFHO_2 + Cl \rightarrow CF_3CFHO + ClO \quad (10)$$

$$2CF_3CFHO_2 \rightarrow 2CF_3CFHO + O_2 \quad (4)$$

Mixtures of $CF_3CFH_2/Cl_2/O_2/N_2$ were prepared and stored in a glass bulb. CF_3CFH_2 of 99% stated purity was procured from Lancaster, and Cl_2 of 99.9% stated purity was supplied by Sigma. The Toll Company supplied extra-dry-grade O_2 and N_2 of 99.9% purity. CF_3CFH_2 and Cl_2 were degassed by freeze−pump−thaw cycles before use.

Results

Determination of k_1/k_2. Experiments were done with gas mixtures consisting of 25 mol % CF_3CFH_2, 15% Cl_2, 1−4% O_2, and N_2 as needed to make up the balance. The experiments were conducted at 20−35 Torr and at 259−297 K. HC(O)F, the decomposition product of reaction 2, was detected as $[HCOF]^+$ at $m/z = 48$. In some experiments, $m/z = 47$ ($[COF]^+$) was monitored. The kinetic results were identical to those from $m/z = 48$, indicating that complications from the fragmentation of other species such as CF_3CFHO and CF_3CFHO_2 are unimportant. Figure 1 shows the kinetic growth of HC(O)F at 273 K and 20 Torr. A plateau is reached after approximately 10 ms, followed by a slow decrease in HC(O)F at times beyond 30 ms (not shown in Figure 1). The decrease is due solely to the purge flow. Figure 1 also shows that the number of counts per flash in the plateau region depends on the partial pressure of O_2; the $[HCOF]^+$ signal decreases as the partial pressure of O_2 increases. This was interpreted as evidence for the increasing competition of O_2 for CF_3CFHO radicals. Experiments at the other temperatures and pressures gave similar HC(O)F growth curves.

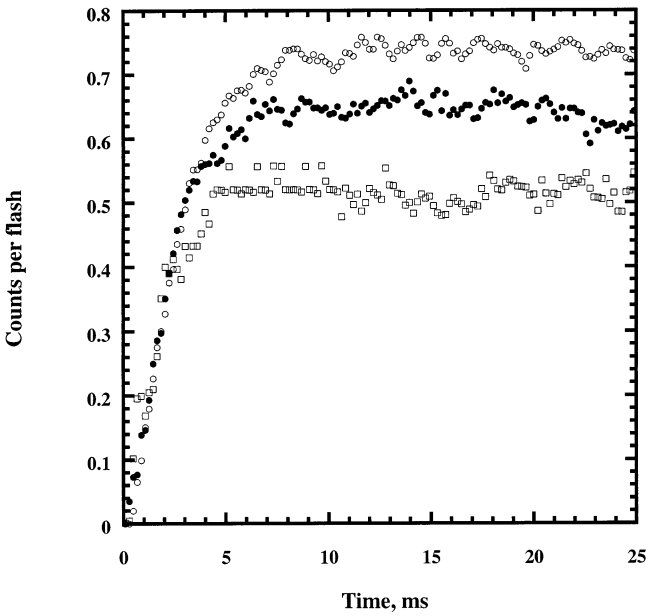

Figure 1. HC(O)F growth curve at 273 K and 20 Torr. Gas mixture: 25% HFC-134a/15% Cl_2/N_2/(○) 1% O_2, (●) 2% O_2, or (□,) 4% O_2.

We were unable to observe the products of reaction 1. The detection of $CF_3C(O)F$ at $m/z = 116$ failed because of the low abundance of this ion in the mass spectrum[18] and the decrease of the signal-to-noise ratio at higher masses in the quadrupole. The fragment ion $[CF_3CO^+]$ is also of low abundance,[18] and $[CF_3^+]$ is obscured by the fragmentation of CF_3CFH_2. The detection of HO_2 at $m/z = 33$ failed, presumably because of the low concentration of this reactive intermediate.

In several of the steady-illumination experiments referenced above, COF_2 formation was observed. We searched for $[COF_2]^+$ at $m/z = 66$ but did not find any signal greater than the background at this mass. If COF_2 were present, then we would have been able to detect it readily.

In the absence of data on $CF_3C(O)F$ formation, it was necessary to use only HC(O)F data to investigate CF_3CFHO radical kinetics. The rate of formation of HC(O)F in these experiments is not well enough separated from the rate of formation of CF_3CFHO to allow the determination of $(k_1 + k_2)$ by fitting the HC(O)F growth curves. However, k_1/k_2 could be obtained from the yield of HC(O)F. The HC(O)F yield was taken to be proportional to the counts per flash in the plateau. The relative yields of HC(O)F determined in pairs of experiments with different pressures of O_2 were used to determine k_1/k_2. The ion counts in the plateau region were reduced by the purge flow in experiments at temperatures higher than 297 K and at pressures lower than 20 Torr. For this reason, the experimental conditions were confined to pressures of 20 and

35 Torr and temperatures from 259 to 297 K to avoid erroneous results caused by the purge flow.

The rate-coefficient ratio, k_1/k_2, was determined from the relative yield of HC(O)F in pairs of experiments in which the only difference was the partial pressure of O_2. If 1 and 2 are the only two reactions competing for CF_3CFHO radicals, then the rate ratio of reactions 1 and 2 can be expressed by eq 11:

$$\frac{[CF_3C(O)F]}{[HC(O)F]} = \frac{k_1[O_2]}{k_2} \qquad (11)$$

A material balance for the total CF_3CFHO formed, integrated over the course of the reaction, is given by eq 12, which can be used to eliminate the unmeasured $CF_3C(O)F$ from eq 11.

$$[CF_3CFHO]_{total} = [CF_3C(O)F]_T + [HC(O)F]_T \qquad (12)$$

In eq 12, $[CF_3C(O)F]_T$ and $[HC(O)F]_T$ are the yields of $CF_3C(O)F$ and HC(O)F. Substitution into eq 11 and obtaining the ratio of the result of pairs of experiments in which all variables except the partial pressure of O_2 are the same gives eq 13.

$$\frac{k_1}{k_2} = \frac{\alpha - P}{P[O_2]_1 - \alpha[O_2]_2} \qquad (13)$$

In eq 13, $P \equiv [HC(O)F]_{1,T}/[HC(O)F]_{2,T}$, $\alpha \equiv [CF_3CFHO]_{1,total}/[CF_3CFHO]_{2,total}$, and subscripts 1 and 2 refer to each experiment of the pair. P is obtained from the counts per flash in the plateau region of HC(O)F versus time plots such as those shown in Figure 1.

The calculation of k_1/k_2 by eq 13 requires the determination of α. If the total number of CF_3CFHO radicals formed is the same in each pair of experiments, then α would be equal to 1, but this is not the case. Although conditions are set to generate equal numbers of Cl atoms in each pair of experiments initially, O_2 competes with HFC-134a for the available Cl atoms,

$$Cl + O_2 + M \rightarrow ClOO + M \qquad (14)$$

and the total amount of CF_3CFHO formed decreases as O_2 increases. Because the rate of reaction 14 is both temperature- and pressure-dependent, α depends not only on the O_2 partial pressure but also on the temperature and total pressure. Because α is a complicated function of reaction chemistry and conditions, it was obtained by a numerical integration of the reaction mechanism in Table 1, which includes other reactions for the removal and generation of Cl atoms. The mechanism is discussed later. To calculate α by simulation, the rates of reactions 1 and 2 were set equal to zero. With no provision in the mechanism for the removal of CF_3CFHO radicals, the predicted CF_3CFHO asymptotically reached a limiting value that could be used for the calculation of α. The values of α obtained in this way are listed in Table 2. In the pair of experiments used for each determination of α, the one labeled 2 had the higher O_2 pressure, making the expected values of $\alpha \geq 1$ if reactions removing Cl are the major factor affecting α. The values of α decreased with decreasing oxygen levels at all conditions, reflecting the decreased competition of O_2 for Cl atoms. The largest values of α were found at the lowest temperatures. This can be largely explained by the negative temperature coefficient of reaction 14 and the positive activation energy of reaction 8. The pressure dependence of α is in accord with the pressure dependence of reaction 14. At higher temperatures, α values are closer to 1 because the temperature dependence of reactions 8 and 14 makes the loss of Cl by reaction with O_2 less significant.

With the values of α from Table 2, k_1/k_2 was calculated by eq 13. Each k_1/k_2 value listed in Table 3 is the average of three values of k_1/k_2 obtained from reactant mixtures in which the mole fractions of O_2 are 1, 2, and 4%, respectively, everything else remaining the same. There are nine experiments at each total pressure and temperature (with different concentrations of O_2). The experiments were repeated at different total pressures and temperatures, and at each condition, the average k_1/k_2 was calculated. The results summarized in Table 3 show that k_1/k_2

TABLE 1: Reaction Model for Numerical Simulations[a]

reaction	k, $cm^3\ s^{-1}$ or s^1	reference
$CF_3CFHO + O_2 \rightarrow CF_3CFO + HO_2$	4.05×10^{-15}	this work
$CF_3CFHO + M \rightarrow CF_3 + HC(O)F + M$	1.27×10^{3}	this work
$Cl + CF_3CFH_2 \rightarrow CF_3CFH + HCl$	7.76×10^{-16}	34
$CF_3CFH + O_2 + M \rightarrow CF_3CFHO_2 + M$	6.2×10^{-12}	13
$CF_3CFH + Cl_2 \rightarrow CF_3CFHCl + Cl$	1.28×10^{-14}	31
$2CF_3CFHO2 \rightarrow 2\ CF_3CFHO + O_2$	3.16×10^{-12}	33
$2CF_3CFHO_2 \rightarrow CF_3C(O)F + CF_3CFHOH + O_2$	3.5×10^{-13}	27
$CF_3CFHO_2 + Cl \rightarrow CF_3CFHO + ClO$	6.6×10^{-12}	30
$CF_3CFHO_2 + ClO \rightarrow CF_3CFHO + ClOO$	4.5×10^{-12}	30
$CF_3 + O_2 + M \rightarrow CF_3O_2 + M$	2.86×10^{-12}	35
$CF_3CFHO_2 + CF_3O_2 \rightarrow CF_3CFHO + CF_3O + O_2$	2.91×10^{-12}	35
$2CF_3O_2 \rightarrow 2CF_3O + O_2$	2.0×10^{-12}	35
$Cl + O_2 + M \rightarrow ClOO + M$	2.49×10^{-15}	35
$Cl + HO_2 \rightarrow O_2 + HCl$	3.45×10^{-11}	35
$2ClO \rightarrow Cl + OClO$	3.17×10^{-15}	35
$2Cl \rightarrow Cl_2$	3.77×10^{-14}	35
$Cl + ClOO \rightarrow O_2 + Cl_2$	2.3×10^{-10}	35
$Cl + ClOO \rightarrow 2ClO$	1.2×10^{-11}	35
$2ClOO \rightarrow$ product(s)	1.6×10^{-11}	36
$ClO + HO_2 \rightarrow O_2 + HOCl$	7.16×10^{-12}	35
$2HO_2 + M \rightarrow O_2 + H_2O_2 + M$	6.02×10^{-14}	35
$2ClO \rightarrow O_2 + Cl_2$	2.16×10^{-15}	35
$Cl + HC(O)F \rightarrow HCl + CFO$	7.28×10^{-16}	5
$CF_3CFH_2 + CF_3O \rightarrow CF_3CFH + CF_3OH$	1.1×10^{-15}	37
$CF_3O_2 + CF_3O \rightarrow CF_3O_3CF_3$	1×10^{-10}	38
$CF_3CFHO_2 + CF_3O \rightarrow CF_3CFHO_3CF_3$	1.79×10^{-11}	37
$CF_3 + Cl_2 \rightarrow CF_3Cl + Cl$	3.5×10^{-14}	39

[a] Rate coefficients quoted at 259 K, 20 Torr.

TABLE 2: Values of $\alpha = [CF_3CFHO]_{1,total}/[CF_3CFHO]_{2,total}$ Determined by Numerical Simulations[a]

		$[O_2]_2\%/[O2]_1\%$		
T (K)	P (Torr)	4%/1%	4%/2%	2%/1%
259	20	1.49678	1.28320	1.16645
	35	1.75994	1.40371	1.25408
265	20	1.40845	1.24069	1.13520
	35	1.63988	1.24069	1.21374
273	20	1.36930	1.22220	1.12032
	35	1.58705	1.33014	1.19318
297	20	1.08921	1.07170	1.01636
	35	1.15955	1.12537	1.03040

[a] Gas mixture: 25% FHC134a/15% Cl_2.

TABLE 3: Experimentally Determined Values of k_1/k_2

T (K)	P (Torr)	$[O_2]$ range (molecule cm^{-3})	k_1/k_2 (cm^3 molecule^{-1})
259	20	$7.659 \times 10^{15}-2.983 \times 10^{16}$	$(3.0 \pm 0.8) \times 10^{-18}$
	35	$1.340 \times 10^{16}-5.221 \times 10^{16}$	$(1.9 \pm 0.4) \times 10^{-18}$
265	20	$7.486 \times 10^{15}-2.916 \times 10^{16}$	$(2.6 \pm 0.9) \times 10^{-18}$
	35	$1.310 \times 10^{16}-5.102 \times 10^{16}$	$(1.3 \pm 0.4) \times 10^{-18}$
273	20	$7.267 \times 10^{15}-2.830 \times 10^{16}$	$(1.3 \pm 0.5) \times 10^{-18}$
	35	$1.272 \times 10^{16}-4.953 \times 10^{16}$	$(8.3 \pm 3.5) \times 10^{-19}$
297	20	$6.679 \times 10^{15}-2.601 \times 10^{16}$	$(4.0 \pm 1.4) \times 10^{-19}$
	35	$1.169 \times 10^{16}-4.553 \times 10^{16}$	$(2.2 \pm 0.9) \times 10^{-19}$

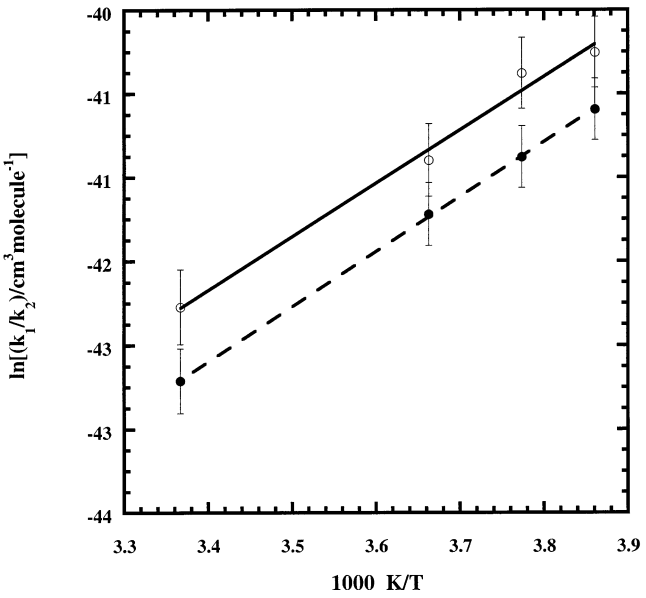

Figure 2. Temperature dependence of k_1/k_2: ○, 20 Torr; ●, 35 Torr.

is both pressure- and temperature-dependent. Because reaction 1 is expected to be pressure-independent, the pressure dependence of k_1/k_2 can be attributed to k_2 and is consistent with reaction 2 being in the unimolecular falloff region. The temperature coefficient of k_1/k_2 at 20 and 35 Torr was determined from a linear least-squares analysis of the Arrhenius plots shown in Figure 2. The Arrhenius expressions are given by eqs 15 and 16.

$$\left[\frac{k_1(T)}{k_2(T)}\right]_{20\text{Torr}} = (2.4 \pm 0.8) \times 10^{-25} e^{(4248\pm550)/T}\ \text{cm}^3\,\text{molecule}^{-1} \quad (15)$$

$$\left[\frac{k_1(T)}{k_2(T)}\right]_{35\text{Torr}} = (9.1 \pm 3.3) \times 10^{-26} e^{(4370\pm500)/T}\ \text{cm}^3\,\text{molecule}^{-1} \quad (16)$$

Ab initio Calculations. Ab initio molecular orbital calculations were made to study the C−C bond scission of CF_3CFHO. The C−F and C−H bond energies are too large for the loss of H or F from CF_3CFHO to occur in the atmosphere. Calculations were made with the Gaussian 98 series of programs on a Silicon Graphics workstation or an IBM SP supercomputer. G2[19] and G2(MP2)[20] theories were used to calculate the total energies of those species. The optimized geometries of the reactant, the products, and the C−C bond rupture transition state were obtained at UHF/6-31G(d) and UMP2(Full)/6-31G(d) levels. For the geometry optimization of the transition-state structure, the QST3[21] option, based on the structures of the reactant, the products, and a guess for the transition state, was used.

The MP2(full)/6-31G(d) optimized geometries of CF_3CFHO, the C−C bond-scission transition state, and the products CF_3 and HC(O)F are listed in Table 4. They are very close to the MP2/6-31G(d,p) optimized structures of the first three species reported by Schneider et al.,[10] but there are differences with the HC(O)F structure. There are also some differences with the bond lengths of CF_3CFHO and $CF_3CFHO^{‡}$ obtained by Somnitz and Zellner[11] from geometry optimizations at UHF/6-31G(d), B3LYP/6-31G(d), and B3LYP/cc-pVTZ levels. The C−C bond lengthening of the transition state is predicted to be 0.38 Å by both of the MO calculations and 0.51 Å by the density functional calculation.[11]

Our calculations show that both the ground state of CF_3CFHO and the transition state for C−C bond scission have asymmetric structures and are ^2A electronic states. The transition state has one imaginary frequency, confirming that the optimized structure is a saddle point. The reaction path following calculations (IRC calculations) at the HF/6-31G(d) level also verified that the transition state is on the path from the CF_3CFHO ground state to the decomposition products, CF_3 and HC(O)F.

The total energies of the reactant, products, and transition state were calculated at the HF/6/31G(d), MP2(full)/6-31G(d), MP2/6-311G(d,p), MP2/6-311+G(d,p), MP2/6-311G(2df,p), MP2/6−311-G(3df,2p), MP4/6-31G(d,p), MP4/6-311+G(d,p), MP4/6-31G(2df,p), and QCISD(T,E4T)/6-311G(d,p) levels of theory and are listed in Table 5. Also in Table 5 are energies obtained by the G2[19] and G2MP2[20] basis set additivity methods.

Zero-point energy corrected barrier heights for C−C bond scission were calculated at each of the theory levels listed in Table 5 and are given in Table 6, along with barrier heights reported by Schneider et al.[10] and Somnitz and Zellner.[11] The barrier heights calculated in this work tend to decrease with increasing basis set size and with the treatment of electron correlation. (See the QCISDT result.) The G2MP2 and G2 barriers at 9.5 kcal mol^{-1}, as far as we are aware, are the lowest yet computed for reaction 2 by high-level calculations. They are 1.2 kcal mol^{-1} lower than the 10.7 kcal mol^{-1} barrier that was also computed by a basis set additivity method[10] and are about 2.6 kcal mol^{-1} beneath the lowest barrier calculated by Somnitz and Zellner.[11]

CI-singles (CIS) calculations for modeling excited states as a combination of single substitutions out of the HF ground state of CF_3CFHO were made. The CIS calculations found, at the

TABLE 4: MP2(full)/6-31G(d) Optimized Geometries of CF_3CFHO, $CF_3CFHO^{‡}$, and Reaction Products

Bond Lengths (Å)

	C_1-C_2	C_1-F_1	C_1-F_2	C_1-F_3	C_2-F_4	C_2-H	C_2-O
CF_3CFHO	1.5308	1.3420	1.3401	1.3411	1.3785	1.1014	1.3428
$CF_3-CFHO^{‡}$	1.9146	1.3184	1.3133	1.3246	1.3750	1.1019	1.2058
CF_3		1.3272	1.3272	1.3272			
HC(O)F					1.3137	1.0808	1.1641

Planar Angles (deg)

	$C_2-C_1-F_1$	$C_2-C_1-F_2$	$C_2-C_1-F_3$	$C_1-C_2-F_4$	C_1-C_2-H	C_1-C_2-O
CF_3CFHO	109.708	110.703	109.982	107.092	109.168	110.539
$CF_3-CFHO^{‡}$	107.310	108.085	106.083	97.124	93.065	101.147
CF_3	F−C−F 111.91					
HC(O)F	F−C−H 110.05	F−C−O 123.02	O−C−H 126.93			

TABLE 5: Total Energies in Hartrees[a]

	CF_3CFHO	$CF_3-CFHO^{\ddagger}$	CF_3	HC(O)F
HF/6-31G(d)	−548.898 125	−548.850 285	−336.131 183	−212.747 841
MP2(full)/6-31G(d)	−549.984 278	−549.954 530	−336.755 762	−213.229 262
MP2/6-311G(d,p)	−550.277 204	−550.250 954	−336.942 274	−213.341 173
MP2/6-311+G(d,P)	−550.303 703	−550.277 383	−336.958 084	−213.352 131
MP2/6-311G(2df,p)	−550.550 671	−550.526 861	−337.108 243	−213.447 496
MP2/6-311+G(3df,2p)	−550.604 701	−550.580 960	−337.140 085	−213.469 857
QCISD(T,E4T)/6-311G(d,p)	−550.336 439	−550.315 160	−336.967 523	−213.365 265
MP4/6-311G(d,p)	−550.339 734	−550.314 082	−336.970 362	−213.369 592
MP4/6-311+G(d,p)	−550.368 904	−550.343 331	−336.987 747	−213.381 252
MP4/6-311G(2df,p)	−550.627 668	−550.604 248	−337.145 051	−213.481 280
G2MP2	−550.732 685	−550.717 554	−337.213 417	−213.518 287
G2	−550.749 821	−550.734 634	−337.223 712	−213.524 352
ZPE[HF/6-31G(d)]	0.040 816	0.036 738	0.013 560	0.023 142
no. of α valence electron	22	22	13	9
no. of β valence electron	21	21	12	9

[a] Scale factor for zero-point energies: 0.8929.

TABLE 6: Energy Barriers for C−C Bond Scission in CF_3CFHO (kcal mol^{-1}) Corrected for Zero-Point Energy

energy level	geometry basis set	energy barrier	reference
HF/6-31G(d)	HF/6-31G(d)	27.73	this work
MP2(full)/6-31G(d)	MP2(full)/6-31G(d)	18.15	this work
MP2/6-311G(d,p)	MP2(full)/6-31G(d)	14.19	this work
MP2/6-311+G(d,p)	MP2(full)/6-31G(d)	14.23	this work
MP2/6-311G(2df,p)	MP2(full)/6-31G(d)	12.66	this work
MP2/6-311+G(3df,2p)	MP2(full)/6-31G(d)	12.61	this work
QCISD(T,4E)/6-311G(d,p)	MP2(full)/6-31G(d)	11.07	this work
MP4/6-311G(d,p)	MP2(full)/6-31G(d)	13.81	this work
MP4/6-311+G(d,p)	MP2(full)/6-31G(d)	13.76	this work
MP4/6-311G(2df,p)	MP2(full)/6-31G(d)	12.41	this work
G2(MP2)	MP2(full)/6-31G(d)	9.50	this work
G2	MP2(full)/6-31G(d)	9.53	this work
B3LYP/6-31G(d,p)	B3LYP/6-31G(d,p)	10.24	this work
CCSD(T)/TZ2P	MP2(full)/6-31G(d,p)	10.7	10
G3((P)MP2)	B3LYP/cc-pVTZ	12.09	11

HF/6-31G(d) level, three excited states with predicted energies of 0.6713, 4.7285, and 9.7953 eV.

Spin contamination is not important for the CF_3CFHO radical because $\langle S^2\rangle$ is in the range of 0.758 at HF/6-31G(d) to 0.76 at QCISD(T)/6-311G(d,p) before annihilation, only slightly larger than the expected value of $\langle S^2\rangle = 0.75$ for doublets. However, for the C−C bond-breaking transition state, $\langle S^2\rangle$ is in the range of 0.873 at QCISD(T)/6-311G(d,p) to 0.894 at HF/6-31G(d).

We estimated the enthalpy of formation of CF_3CFHO at 298 K from the thermally corrected G2 and G2(MP2) energies of CF_3CFHO and the elements from which the oxy radical is formed. The calculations give $\Delta H°_{f298}(CF_3CFHO) = -203.0$ kcal mol^{-1} at G2MP2 and $\Delta H°_{f298}(CF_3CFHO) = -203.4$ kcal mol^{-1} at G2. Also, $\Delta H°_{f0}(CF_3CFHO) = -195.8$ kcal mol^{-1}at G2MP2, and $\Delta H°_{f0}(CF_3CFHO) = -196.1$ kcal mol^{-1}at G2. The 298 K values are in excellent agreement with $\Delta H°_{f298}(CF_3CFHO) = -203$ kJ mol^{-1} determined by Dixon and Wiley.[22]

RRKM Calculations. An RRKM model was obtained from moments of inertia and vibrational frequencies derived from the MP2(full)/6-31G(d) optimized structures and a critical energy, $E_{2,0}$, set equal to the 9.53 kcal mol^{-1} G2 barrier. The frequencies and moments of inertia are listed in Table 7. The UNIMOL[23] Fortran program package, with a tight transition-state treatment, was used for calculations of $k(E)$. The moments of inertia and rotational constants were obtained using the GEOM program.[24] Master equation calculations were made using the biased random-walk model for energy transfer[25] to calculate $k_2(T)$. Lennard-Jones parameters were obtained via the combining rules $\sigma_{AB} = (\sigma_A + \sigma_B)/2$ and $\epsilon_{AB} = (\epsilon_A \times \epsilon_B)^{1/2}$.[26] The bath gas used in this work is typically a mixture of 25% HFC-134a/15% Cl_2/60% N_2. Lennard-Jones diameters were estimated according to Hirschfelder, Curtiss, and Bird,[27] and $\sigma_{CF_3CFHO} = 5.2$ Å and $\sigma_{bath\ gas} = 4.39$ Å were obtained. $\epsilon_{CF_3CFHO} = 250$ K was taken from Schneider et al.[10] $\epsilon_{bath\ gas} = 161$ K was estimated from the above combining rule. This RRKM model is called model I.

Model I calculations of k_2 with full angular momentum conservation at several pressures of interest are listed in Table 8. The low- and high-pressure limiting rate coefficients $k_{2,0}(T)$ $k_{2,\infty}(T)$, calculated over the temperature range of 259−297 K, are given by eqs 17 and 18.

$$k_{2,0}(T) = 1.01 \times 10^{-7} e^{-4078/T}\ \text{cm}^3\ \text{molecule}^{-1}\ \text{s}^{-1} \quad (17)$$

$$k_{2,\infty}(T) = 5.90 \times 10^{13} e^{-5260/T}\ \text{s}^{-1} \quad (18)$$

RRKM predictions of the temperature dependence of k_2 at 20 and 35 Torr are given by eqs 19 and 20.

$$k_2(T)_{\text{cal,20 Torr}} = 3.67 \times 10^{10} e^{-4006/T}\ \text{s}^{-1} \quad (19)$$

$$k_2(T)_{\text{cal,35 Torr}} = 6.89 \times 10^{10} e^{-4068/T}\ \text{s}^{-1} \quad (20)$$

Figure 3 shows the pressure dependence of $k_2/k_{2,\infty}$ at 273 K, illustrating that the experimental data at 20 and 35 Torr are well into the unimolecular falloff and that the falloff region is exceptionally broad. The breadth is attributable mainly to the small barrier height for C−C bond breaking.

The above RRKM calculations are based on the 25% HFC-134a/15% Cl_2/60% N_2 bath gas used in this work. RRKM calculations were also made using N_2 as the bath gas to determine if significant changes would result. The results are listed in the Table 8. Using the N_2 bath gas affects k_2 only slightly, and a consideration of bath gas effects will have very little influence on atmospheric modeling.

Maricq and Szente[8] reported the temperature dependence (216−372 K) of the CF_3CFHO dissociation rate coefficient at 230 Torr, taken from observations of the time dependence of a transient UV absorption feature attributed to CF_3CFHO. The data were expressed in Arrhenius form by $k_2(T)_{230\ \text{Torr}} = (3.7 \pm 0.7) \times 10^7 e^{(-2200\pm150)/T}\ \text{s}^{-1}$. The preexponential factor and activation energy in this Arrhenius expression are considerably smaller than the corresponding 230 Torr A_2 and E_2 that can be obtained from any of the existing RRKM models. Nevertheless, Table 9 shows that the individual rate coefficients calculated from this expression at 259, 273, and 295 K are in reasonable accord with the k_2 calculated from the Schneider et al.[10] RRKM

TABLE 7: Calculated Vibrational Frequencies, Moments of Inertia, and Rotational Constants

Unscaled Vibrational Frequencies (cm^{-1})

CF_3CFHO (ground state)
77, 222, 241, 372, 410, 520, 577, 595, 710, 860, 1078, 1153, 1214, 1280, 1332, 1343, 1396, 3070.

$CF_3-CFHO^{\ddagger}$
904 i, 57, 170, 206, 287, 347, 522, 537, 628, 658, 890, 1053, 1149, 1337, 1376, 1391, 1674, 3071

Principal Moments of Inertia ($Å^2$)

CF_3CFHO (ground state)
244.449, 201.568, 137.565

$CF_3-CFHO^{\ddagger}$
260.078, 219.335, 137.574

Rotational Constants (cm^{-1})

CF_3CFHO (ground state)
0.06889, 0.08355, 0.1224

$CF_3-CFHO^{\ddagger}$
0.06475, 0.07678, 0.1224

TABLE 8: RRKM Calculations[a]

Bath Gas: 25% HFC-134a/15% Cl_2/60% N_2, Barrier Height = 9.53 kcal mol^{-1}

	259 K	265 K	273 K	297 K
$k_{2,20\ Torr}$ (s^{-1})	6.99×10^3	1.00×10^4	1.58×10^4	5.07×10^4
$k_{2,35\ Torr}$ (s^{-1})	1.03×10^4	1.49×10^4	2.35×10^4	7.72×10^4
$k_{2,760\ Torr}$ (s^{-1})	4.72×10^4	7.11×10^4	1.19×10^5	4.56×10^4
$k_{2,0}$[b]	1.46×10^{-14}	2.11×10^{-14}	3.34×10^{-14}	1.10×10^{-13}
$k_{2,\infty}$ (s^{-1})	8.94×10^4	1.41×10^5	3.52×10^5	1.20×10^6
β_2	0.391	0.382	0.373	0.332

$k_{2,0}(T) = 1.01 \times 10^{-7} e^{-4078/T}$ cm^3 $molecule^{-1}$ s^{-1}
$k_{2,\infty}(T) = 5.90 \times 10^{13} e^{-5260/T}$ s^{-1}

Bath Gas: 25% HFC-134a/15% Cl_2/60% N_2, Barrier Height = 10.7 kcal mol^{-1}

	259 K	265 K	273 K	297 K
$k_{2,20\ Torr}$ (s^{-1})	1.27×10^3	1.94×10^3	3.28×10^3	1.29×10^4
$k_{2,35\ Torr}$ (s^{-1})	1.79×10^3	2.74×10^3	4.67×10^3	1.88×10^4
$k_{2,760\ Torr}$ (s^{-1})	6.29×10^3	1.01×10^4	1.82×10^4	8.64×10^4
$k_{2,0}$[b]	3.52×10^{-15}	5.35×10^{-15}	9.00×10^{-15}	3.52×10^{-14}
$k_{2,\infty}$ (s^{-1})	9.69×10^3	1.61×10^4	3.07×10^4	1.73×10^5
β_2	0.406	0.396	0.384	0.347

$k_{2,0}(T) = 2.25 \times 10^{-7} e^{-4653/T}$ cm^3 $molecule^{-1}$ s^{-1}
$k_{2,\infty}(T) = 5.91 \times 10^{13} e^{-5836/T}$ s^{-1}

Bath Gas: N_2, Barrier Height = 10.7 kcal mol^{-1}

	259 K	265 K	273 K	297 K
$k_{2,20\ Torr}$ (s^{-1})	1.32×10^3	2.01×10^3	3.41×10^3	1.35×10^4
$k_{2,35\ Torr}$ (s^{-1})	1.85×10^3	2.83×10^3	4.84×10^3	1.96×10^4
$k_{2,0}$[b]	3.69×10^{-15}	5.61×10^{-15}	9.46×10^{-15}	3.72×10^{-14}
$k_{2,\infty}$ (s^{-1})	9.69×10^3	1.61×10^4	3.07×10^4	1.73×10^5
β_2	0.406	0.396	0.384	0.347

$k_{2,0}(T) = 2.49 \times 10^{-7} e^{-4665/T}$ cm^3 $molecule^{-1}$ s^{-1}
$k_{2,\infty}(T) = 5.91 \times 10^{13} e^{-5836/T}$ s^{-1}

[a] This work. [b] cm^3 $molecule^{-1}$ s^{-1}.

model, which is called model II here. A closer examination of the experimental k_2 shows that they are somewhat larger than the model II calculation at 259 K and somewhat smaller at 295 K, showing why the A_2 and E_2 from the experiments are unusually small. It is expected that an RRKM model with an appropriate barrier would predict reliable Arrhenius parameters at any pressure in the falloff. The 50 mbar (37.5 Torr), 295 K rate coefficient, $k_2 = 1.8 \times 10^4$ s^{-1}, reported by Bednarik et al.[5] is also in better agreement with model II than with the Somnitz and Zellner[11] RRKM model (called model III) or with model I. Table 9 shows that the k_2 values from our G2-derived RRKM model are a factor of 5 to 10 larger than the experimental k_2 and that the Somnitz and Zellner[11] k_2 values (not shown) are about a factor of 10 smaller than the experimental values.

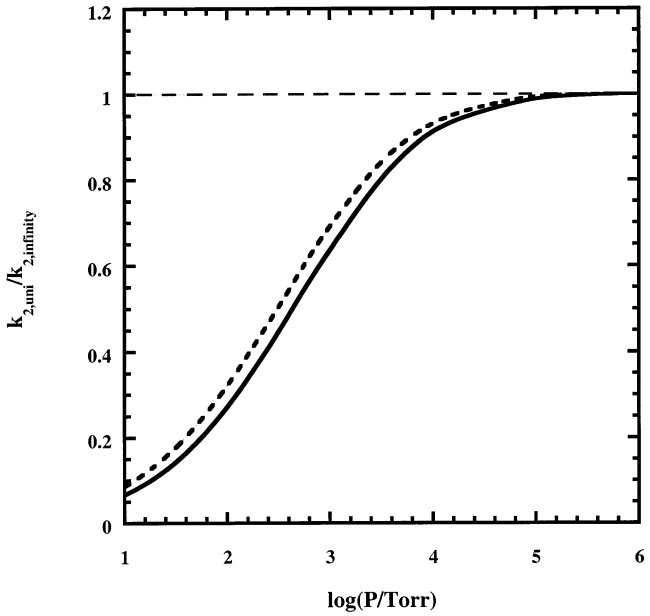

Figure 3. Calculated pressure dependence of $k_{2,uni}/k_{2,\infty}$ at 273 K: - - -, $E_{2,0} = 11.2$ kcal mol^{-1}; —, $E_{2,0} = 10.7$ kcal mol^{-1}.

Discussion

Relative Rate Coefficient k_1/k_2. Equation 15 gives a 20 Torr value of k_1/k_2 that is in agreement with that of Wallington et al.[1], who determined the pressure dependence of k_1/k_2 at 297 K. From their Figure 5, it can be estimated that at 20 Torr $k_1/k_2 \approx 3 \times 10^{-19}$ cm^3, and eq 15 gives $k_1/k_2 = (3.9 \pm 1.3) \times 10^{-19}$ cm^3 at 297 K. Equation 15 is also in agreement with a study of the pressure dependence of k_1/k_2 at 269 and 296 K,[7] where the data have been fit by the Troe method.[28] We calculated $k_1/k_2(269\ K)_{20\ Torr} = (1.4 \pm 0.7) \times 10^{-18}$ cm^3 $molecule^{-1}$ and $k_1/k_2(296\ K)_{20\ Torr} = (2.5 \pm 1.3) \times 10^{-19}$ cm^3 $molecule^{-1}$ from the reported[7] Troe parameters. The 269 K ratio is in good agreement with $k_1/k_2(269\ K)_{20\ Torr} = (1.8 \pm 0.7) \times 10^{-18}$ cm^3 $molecule^{-1}$ from eq 15, and the experimental uncertainty of the 296 K ratio overlaps the uncertainty of $k_1/k_2(296\ K)_{20\ Torr} = (4.2 \pm 1.6) \times 10^{-19}$ cm^3 $molecule^{-1}$ from eq 15.

Equation 16 gives 35 Torr values of k_1/k_2 that are in agreement with the Troe fits reported by Wallington et al.[7] For example, at 297 K eq 16 gives 2.2×10^{-19} cm^3 $molecule^{-1}$, and the Troe expression gives 2×10^{-19} cm^3 $molecule^{-1}$. Equation 16 also gives a 35 Torr value of k_1/k_2 that is in agreement with the experimental value of Bednarik et al.[5] These workers fit transient OH and NO_2 concentration profiles obtained

TABLE 9: Comparison of k_1/k_2, k_2, and k_1

	259 K	273 K	295 K	reference
$(k_1/k_2)_{760\ Torr}$ (cm^3 $molecule^{-1}$)	2.51×10^{-19}	1.23×10^{-19}	4.63×10^{-20}	7
$(k_1/k_2)_{20\ Torr}$ (cm^3 $molecule^{-1}$)	3.2×10^{-18}	1.4×10^{-18}	4.3×10^{-19}	this work
$(k_1/k_2)_{35\ Torr}$ (cm^3 $molecule^{-1}$)	1.9×10^{-18}	8.3×10^{-19}	2.4×10^{-19}	this work
$(k_1/k_2)_{760\ Torr}$ (cm^3 $molecule^{-1}$)	5.9×10^{-19}	2.3×10^{-19}	6.0×10^{-20}	this work[a]
	4.5×10^{-19}	1.7×10^{-19}	4.5×10^{-20}	this work[b]
$k_{2,230\ Torr}$ (s^{-1})	5.75×10^3	1.17×10^4	2.13×10^4	8
	4.35×10^3	1.21×10^4	4.78×10^4	this work[a]
	2.96×10^4	7.15×10^4	2.32×10^5	this work[b]
$k_{2,37.5\ Torr}$ (s^{-1})			1.8×10^4	4
			1.77×10^4	this work[a]
			7.38×10^4	this work[b]
k_1 (cm^3 $molecule^{-1}$ s^{-1})			2.7×10^{-15}	4
	4.05×10^{-15}	4.25×10^{-15}	4.75×10^{-15}	this work[a]
	2.22×10^{-14}	2.03×10^{-14}	1.86×10^{-14}	this work[b]

[a] Scaled with model II ($E_{2,0} = 10.7$ kcal mol^{-1}). [b] Scaled with model I ($E_{2,0} = 9.5$ kcal mol^{-1}).

experimentally from the 351-nm flash photolysis of $CF_3CFH_2/O_2/NO/Cl_2$ mixtures by a numerical simulation of a reaction mechanism. The authors reported $k_1/k_2 = (1.5 \pm 0.3) \times 10^{-19}$ cm^3 at 38 Torr and 295 K. Using eq 16 to calculate k_1/k_2 at 295 K and 35 Torr and linearly extrapolating to 38 Torr gives $k_1/k_2 = (2.1 \pm 0.7) \times 10^{-19}$ cm^3. The two values agree to within experimental uncertainty. Bednarik et al.[5] produced CF_3CFHO by the CF_3CFHO_2 plus NO reaction, which is thought to form chemically activated CF_3CFHO.[7,13] However, chemically activated CF_3CFHO is expected to decompose considerably faster than the millisecond times of the experimental transients, which must be due only to thermal reactions.

The 20 and 35 Torr experimental values of k_1/k_2 were scaled to 760 Torr via eq 21 for comparison with k_1/k_2 calculated from eq 3, assuming that k_1 is independent of pressure.

$$\left(\frac{k_1}{k_2}\right)_{760\ Torr} = \left(\frac{k_1}{k_2}\right)_{P,\text{experimental}} \times \frac{k_{2,P\ (RRKM)}}{k_{2,760\ Torr\ (RRKM)}} \quad (21)$$

The results are presented in Table 9. There is excellent agreement with k_1/k_2 calculated from eq 3 at 295 K and reasonable agreement at 273 K when model I rate coefficients are used. However, at 259 K the scaling results in a k_1/k_2 value that is 80% larger than k_1/k_2 from eq 3. Table 9 also shows that scaling with model II does not agree as well with the 760 Torr data as scaling with model I and that the scaled 259 K value of k_1/k_2 in this case is larger than the data by more than a factor of 2.

The Arrhenius-like expressions for k_1/k_2 can also be used in eq 21. With model I, scaling eq 15 gives $(k_1/k_2)_{760\ Torr} = 3.8 \times 10^{-27}e^{4827/T}$ cm^3, and scaling eq 16 gives $(k_1/k_2)_{760\ Torr} = 2.7 \times 10^{-27}e^{4887/T}$ cm^3. There is a significant discrepancy between these two expressions and eq 3. It is evident that this is caused by the stronger temperature dependence of k_1/k_2 data at 20 and at 35 Torr compared with the 760 Torr data. The discrepancy is almost entirely because of the differences in the 259 K data.

Estimates of $k_1(T)$. An estimate of $k_1(T)$ was made by multiplying the temperature dependence of k_1/k_2 from eqs 15 and 16 by the RRKM-calculated $k_2(T)$ expressed by eqs 19 and 20, respectively. The estimate with the 20 Torr data is $k_1(T) = (8.8 \pm 2.9) \times 10^{-15}e^{(242\pm550)/T}$ cm^3 $molecule^{-1}$ s^{-1}, and with the 35 Torr data it is $k_1(T) = (6.3 \pm 2.3) \times 10^{-15}e^{(302\pm500)/T}$ cm^3 $molecule^{-1}$ s^{-1}, where the uncertainties are those associated with the experimental measurements. The two expressions for k_1 agree to within the experimental uncertainty and show no evidence for a pressure dependence of k_1. Averaging these two k_1 estimates gives

$$k_1(T) = (7.5 \pm 2.5) \times 10^{-15}e^{(272\pm500)/T}\ cm^3\ molecule^{-1}\ s^{-1} \quad (22)$$

If the model I calculated temperature dependence of k_2 at 760 Torr is applied to eq 3, then k_1 is estimated to be

$$k_1(T) = (4.87^{+3.1}_{-2.1}) \times 10^{-13}e^{(-960\pm150)/T}\ cm^3\ molecule^{-1}s^{-1} \quad (23)$$

The different temperature dependencies of k_1 in eqs 23 and 22 originate in the differences in the exponents of eqs 3, 15, and 16. The reasons for the different temperature dependencies of k_1/k_2 are the differences in the low-temperature data. Although the Arrhenius parameters in eqs 22 and 23 are different, the temperature dependence is not strong and the temperature range is not large, so the individual k_1 values are not very different. At 295 K, $k_1 = 1.9 \times 10^{-14}$ cm^3 $molecule^{-1}$ s^{-1} is calculated from both eqs 22 and 23. Using eq 22, k_1 increases by only 13% from 295 to 259 K, and k_1 from eq 23 decreases by 30% over the same range. All of the k_1 values estimated between 295 and 259 K from eqs 22 and 23 are encompassed by $k_1 = (1.8 \pm 0.6) \times 10^{-14}$ cm^3 $molecule^{-1}$ s^{-1}. The range of k_1 about the central value is about the same as the experimental uncertainty in the k_1/k_2 values from which they are derived, so this temperature-independent value suffices over the temperature range of this work.

The rate coefficient of reaction 1 can also be estimated by applying model II to eq 3. From the parameters reported in ref 10, we calculated $k_2(760\ Torr) = 4.8 \times 10^{12}e^{-5296/T}$ s^{-1}, resulting in

$$k_1(T) = 1.2 \times 10^{-12}e^{-1670/T}\ cm^3\ molecule^{-1}\ s^{-1} \quad (24)$$

This preexponential factor differs from the surprisingly large $A_1 \approx 1.4 \times 10^{-11}$ cm^3 $molecule^{-1}$ s^{-1}, estimated by Schneider et al.[10] This value was obtained by scaling A_2 from 760 Torr to the high-pressure limit by applying the factor of 1.4 suggested by Wallington et al.[1]. Comparing the RRKM A_2 at 760 Torr with $A_{2\infty} = 4.8 \times 10^{13}$ s^{-1}, we find that the reaction is actually substantially into the falloff and that the scale factor for A_2 should be about 10. The A_1 obtained by this latter scaling is in reasonable agreement with the A factor in eq 24. However, scaling only the A factor is not very accurate because it ignores the pressure dependence of the activation energy in the falloff. The individual k_1 values calculated from eq 24 are listed in Table 9. They are seen to be a factor of about 5 to 10 smaller than the k_1 values estimated from model I. According to eq 24, k_1 increases by less than 20% between 259 and 295 K, and $k_1 = (4.35 \pm 0.3) \times 10^{-15}$ cm^{-3} $molecule^{-1}$ s^{-1} covers the entire range.

Bednarek et al.[5] reported $k_1 = (2.7^{+2.7}_{-1.4}) \times 10^{-15}$ cm^3 $molecule^{-1}$ s^{-1} from numerical simulation of their 295 K data. Rattigan et al.[4] combined the Bednarek et al.[5] rate coefficient with the recommended A factor for the ethoxy plus O_2 reaction,[29] 6.0×10^{-15} cm^3 $molecule^{-1}$ s^{-1}, to obtain $k_1(T) = 6.0 \times 10^{-14}e^{-925/T}$ cm^3 $molecule^{-1}$ s^{-1}. This expression gives k_1 values that compare favorably with the individual k_1 values in Table 9 estimated using model II, whereas the k_1 values estimated using model I are about a factor of 5 larger. Somnitz and Zellner[11] recommended $k_1 = 4.2 \times 10^{-16}$ cm^3 $molecule^{-1}$ s^{-1} at 295 K.

This comparatively smaller rate coefficient comes from model III calculations, which give smaller k_2 values and therefore smaller k_1 when combined with k_1/k_2 from eq 3. Because the various estimated absolute values of k_2 and k_1 are at variance by about a factor of 40, we next carried out numerical simulations of the experimental HC(O)F growth curves to determine which estimates of k_1 and k_2 would best simulate the data.

Mechanism. The mechanism for the numerical simulations is listed in Table 1. All of the rate coefficients except those for the reaction of Cl and ClO with CF_3CFHO_2 are available from literature reports. In the absence of rate data for these reactions, their rate coefficients were set equal to those for similar reactions of Cl and ClO with $CF_2ClCH_2O_2$.[30] The simulations were only modestly sensitive to these two rate coefficients. When they were varied by ±50%, the simulated HC(O)F growth curves changed by less than the error limits of the data points. Because the unavailability of authentic samples of HC(O)F prevented the calibration of the mass spectrometer, all comparisons were made by scaling to an HC(O)F yield of 1.0 in the plateau. The evaluation of k_1 and k_2 was therefore based on a comparison of the simulations with experiment in the rising portion of the HC(O)F growth curve.

The simulations predict that Cl atoms decay to 1% of their initial concentration in 10 ms and to 0.02% in 20 ms. The following reactions are the principal ones removing Cl.

$$Cl + CF_3CFH_2 \rightarrow CF_3CFH + HCl \quad (8)$$

$$Cl + CF_3CFHO_2 \rightarrow CF_3CFHO + ClO \quad (10)$$

$$Cl + O_2 + M \rightarrow ClOO + M \quad (14)$$

$$Cl + HO_2 \rightarrow O_2 + HCl \quad (25)$$

The relative rates at 259 K and 20 Torr are $r_8/r_{10}/r_{14}/r_{25}$ = 1:0.40:0.27:0.01. Other Cl removal reactions listed in Table 1 have smaller rates than reaction 25. The numerical simulation also revealed that eq 10 is the most important reaction for oxy radical formation. The average rate of reaction 10 between 0 and 30 ms was calculated to be 9 times the average rate of reaction 4 over the same time period.

The reaction of CF_3CFH with Cl_2 regenerates Cl atoms, some of which react with CF_3CFH_2.

$$CF_3CFH + Cl_2 \rightarrow CF_3CFClH + Cl \quad (26)$$

$$Cl + CF_3CFH_2 \rightarrow CF_3CFH + HCl \quad (8)$$

There is the potential for a chain reaction composed of reactions 8 and 26, with CF_3CFH as a chain carrier. Under the conditions of this work, $r_{26} \approx 10r_8$. The principal chain-termination step is reaction 9. With $k_{26}/k_9(\pm 18\%) = 0.16\ e^{(-940/T)}$,[31] the kinetic chain length, which is given by the ratio of the rate of propagation to termination, r_{26}/r_9, varies from 0.01 to 0.04 over the entire range of experimental conditions, and a chain reaction cannot be sustained. This conclusion is supported by experimental observations. In some experiments, the transient HCl signal was monitored and found to reach a plateau after about 15−20 ms. If the chain reaction were important, then HCl would not be expected to become constant but to continue to grow with increasing time as Cl atoms continue to attack CF_3CFH_2. Similarly, the chain would cause HC(O)F to continue to grow, whereas Figure 1 shows this not to be the case.

The CF_3 radical formed by reaction 2 can react with CF_3CFH_2, Cl_2, and O_2, with the addition of O_2 being the dominant reaction. Abstraction of H from CF_3CFH_2 by CF_3 is about 10^{-5} times smaller than the rate of CF_3O_2 formation, and reaction with Cl_2 can account for between 7 and 26% of CF_3 consumption, depending on conditions. The CF_3O_2 radical can react with CF_3CFHO_2 to form additional CF_3CFHO, and it can also disproportionate (reaction 29).

$$CF_3 + O_2 \rightarrow CF_3O_2 \quad (27)$$

$$CF_3CFHO_2 + CF_3O_2 \rightarrow CF_3CFHO + CF_3O + O_2 \quad (28)$$

$$CF_3O_2 + CF_3O_2 \rightarrow CF_3O + O_2 \quad (29)$$

The numerical simulations showed that reactions 27−29 play a minor role in the sense that k_1/k_2 is very insensitive to them. The CF_3O formed by reactions 28 and 29 is removed primarily by association with CF_3O_2 to form a trioxide.[1,3,32] The reaction of CF_3O with CF_3CFH_2 is too slow for the formation of CF_3OH to be important during our 20−30 ms observation time. Because CF_3OH has been suggested to be a precursor of the CF_2O that has been observed in steady photolysis experiments,[5] our failure to observe CF_2O, as noted above, must be due to the successful competition of CF_3O_2 with CF_3CFH_2 for CF_3O. There is no evidence for the removal of HC(O)F by chemical reaction(s) at observation times in the plateau region (Figure 1).

Numerical Simulations. The HC(O)F kinetic growth curves were numerically simulated with the mechanism in Table 1. The rate coefficient, k_2, for the thermal decomposition of CF_3CFHO was calculated from RRKM models. Either model I, model II, or model III was used. Model I with a QCISD(T) barrier of 11.07 kcal mol^{-1} was also used in a few calculations. For consistency, k_1 was constrained to agree with the experimentally determined k_1/k_2 obtained from the plateau of the growth curve being simulated. Thus, k_1 was calculated by $k_1 = (k_1/k_2)_{experimental} \times k_{2,RRKM}$ for each of the RRKM models. The remaining rate coefficients were taken from the literature. No rate coefficients were adjusted to force a fit with the data. The results from the numerical simulations are presented in Figures 4 and 5. The initial concentration of atomic chlorine, $[Cl]_0$, used in the simulations was taken from an experimental determination of this quantity by NOCl actinometry.[30] For these simulations, $[Cl]_0 = 5.6 \times 10^{13}$ molecule cm^{-3} and $[O_2] = 2.98 \times 10^{16}$ molecule cm^{-3}.

At 259 K and 20 Torr, the simulations shown in Figure 4 reveal that the predicted HC(O)F growth rate is RRKM model sensitive. The dominant model parameter is $E_{2,0}$, the ZPE corrected barrier height. Model I ($E_{2,0}$ = 9.53 kcal mol^{-1}) predicts a HC(O)F growth curve that rises slightly faster than the data (open circles), but the 11.07 kcal mol^{-1} QCISD(T) barrier underestimates the growth rate. Model II ($E_{2,0}$ = 10.7 kcal mol^{-1}) fits the growth curve quite well, but model III ($E_{2,0}$ = 12.09 kcal mol^{-1}) underestimates the HC(O)F growth rate. Figure 5a shows that at 273 K model III still does not give a large enough CF_3CFHO radical decomposition rate to predict the observed HC(O)F growth, but the predictions from the other three calculations agree well with the data and are nearly indistinguishable from one another. At 297 K (Figure 5b), the CF_3CFHO decomposition rates calculated by all of the models have become fast enough to agree with the observed HC(O)F growth rate.

The numerical simulations predict that the rate of formation of CF_3CFHO at 259 K is somewhat faster than its decomposition. At this temperature, there is enough separation between these two rates to show the slight overestimation of the observed HC(O)F growth rate by model I. At 273 K, CF_3CFHO

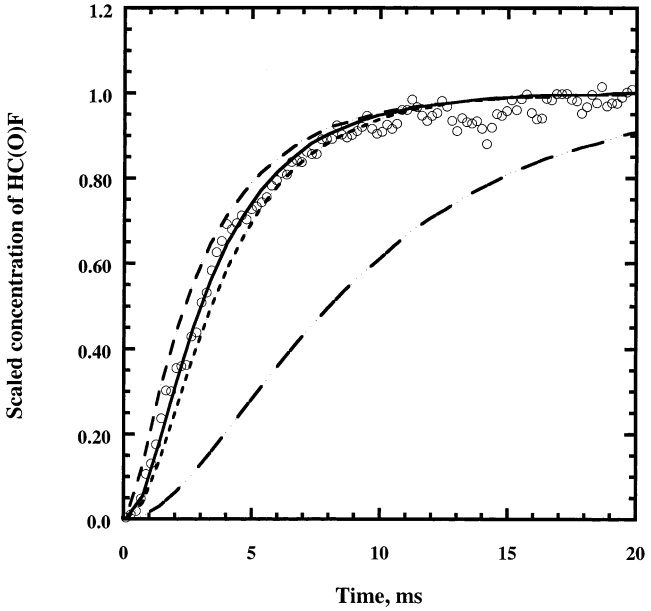

Figure 4. HC(O)F concentration profiles at 259 K and 20 Torr: ○, Experimental data; − − −, model I; —, model II; − · −, model III; - - -, model I calculated with $E_{2,0} = 11.07$ kcal mol^{-1}. Conditions: [HFC134a] = 1.86×10^{17} molecule cm^{-3}; [O_2] = 2.98×10^{16} molecule cm^{-3}; [Cl_2] = 1.12×10^{17} molecule cm^{-3}; [Cl]$_0$ = 5.6×10^{13} molecule cm^{-3}.

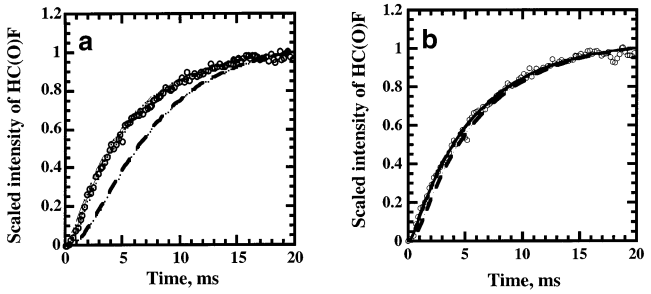

Figure 5. (a) HC(O)F concentration profiles at 273 K and 20 Torr: data and RRKM calculations; − · −, model III. (b) HC(O)F concentration profiles at 297 K and 20 Torr: data and RRKM calculations; − · −, model III.

decomposition rates are faster, and HC(O)F formation is sufficiently rate-limited by CF_3CFHO formation that the overestimation of the HC(O)F growth rate is no longer observable. Furthermore, discrimination between models with $E_{2,0} \leq 11$ kcal mol^{-1} is not possible. At 297 K, it is not possible to discriminate between any models with $E_{2,0} \leq 12$ kcal mol^{-1}.

Conclusions

Model II gives better agreement with both the HC(O)F formation data and the experimentally determined values of k_2,[5,8] as discussed above, than does model I. However, using model I to scale the 20 and 35 Torr k_1/k_2 data to 760 Torr gives better agreement with the 760 Torr data[12] than does scaling with model II. Thus, both models I and II agree with at least part of the existing body of experimental data, and an unambiguous choice between them is difficult at present. Model III is not as satisfactory as either I or II. The difference in the barrier height of models I and II is within the 1.21 kcal mol^{-1} average absolute deviation from experiment that has been found for the G2 method,[20] and it must be concluded that G2 functions as well as expected for the CF_3CFHO radical. We have previously found that G2 works satisfactorily for CH_2ClO radicals, predicting a barrier for HCl elimination that is within 0.5 kcal mol^{-1} of experiment.[40] The basis set additivity method used by Schneider et al.[10] for their model must also be judged to be very satisfactory for CF_3CFHO. It seems most likely then that the barrier for C−C bond scission in CF_3CFHO lies in the range of 9.5 to 10.7 kcal mol^{-1}. For atmospheric modeling, an RRKM model based on MP2/6-31G(d) or MP2/6-31G(d,p) geometry optimizations and a barrier of 9.6 ± 0.6 kcal mol^{-1} will give the best current estimate of k_2.

In Table 9, the values of k_1 from 259 to 295 K obtained from eq 3 and the model II-calculated k_2 at 760 Torr are all encompassed by $k_1 = (4.40 \pm 0.35) \times 10^{-15}$ cm^3 molecule^{-1} s^{-1}. Model II applied to eqs 15 and 16 will give nearly the same result. As shown above, values of k_1 from 259 to 295 K are all encompassed by $k_1 = (1.8 \pm 0.6) \times 10^{-14}$ cm^3 molecule^{-1} s^{-1} when they are obtained from model I and the 20 and 35 Torr k_1/k_2 data. The k_1 values from model I are larger than those from model II primarily because of the lower barrier in the former model. Also, k_1 values obtained from the application of model III to the data are smaller than from either model I or model II because of the higher barrier. For alkoxy radicals, Atkinson[41] has recommended $k(RO + O_2) = 4.0 \times 10^{-19} n \exp(-0.28\ \Delta H_r)$ cm^3 molecule^{-1} s^{-1}, where n is the number of H atoms on the carbon α to the O atom. With ΔH_r (rxn 1) = −38.7 kcal mol^{-1}, from the G2 calculation of $\Delta H_f°(CF_3CFHO)$ and literature data, $k_1(298\ K) = 2 \times 10^{14}$ cm^3 molecule^{-1} s^{-1} is predicted. This is in excellent agreement with the k_1 derived from model I, but it has not been possible to test whether Atkinson's equation is applicable to CF_3CFHO or to halogenated alkoxy radicals in general because of the lack of data, and the agreement cannot be used to support the larger k_1.

In the atmosphere, the relative rate of the reaction of CF_3CFHO with O_2 and thermal decomposition, $r_1/r_2 = k_1[O_2]/k_2$, increase with increasing altitude because k_2 decreases more rapidly with pressure and temperature than does [O_2]. The formation of $CF_3C(O)F$ therefore becomes increasingly important with increasing altitude. At ground level (288 K, 760 Torr), $r_1/r_2 = 0.36$, and at 5 km (253 K, 400 Torr), $r_1/r_2 = 3.8$. The temperatures and pressures are those of the U.S. standard atmosphere.[42] The ground-level calculation uses eq 3, and the 5-km calculation uses $k_1 = 4.35 \times 10^{-15}$ cm^3 molecule^{-1} s^{-1} and RRKM model II. With model I and $k_1 = 1.2 \times 10^{-14}$ cm^3 molecule^{-1} s^{-1}, $r_1/r_2 = 1$ is predicted at 5 km. At 21 km (220 K, 35 Torr),[43] eq 16 predicts $r_1/r_2 = 12$. The extrapolation of eq 16 from the 259 to 297 K range over which it was determined to 220 K causes some uncertainty in the 21-km ratio, but not enough to reverse the upward trend of r_1/r_2 with altitude.

Chemically activated CF_3CFHO is formed by the reaction of CF_3CFHO_2 with NO,[7] and 60% of the oxy radicals formed in this reaction undergo prompt C−C bond rupture.[7,10] The remaining 40% are collisionally stabilized and react thermally. Using the above rate ratios, we calculate that of the CF_3CFHO formed in the atmosphere by the NO reaction the sum of decomposition by prompt and thermal decomposition is 90% at the earth's surface, 68% at 5 km (80% if model I is used), and 63% at 21 km. Because CF_3CFHO is produced in the atmosphere by other paths, such as $CF_3CFHO_2 + HO_2$ and $2CF_3CFHO_2$, which are not exothermic enough to generate chemically activated CF_3CFHO radicals, the percent decomposition will be smaller, and the yield of $CF_3C(O)F$ will be somewhat larger than that implied by the above values.

Acknowledgment. This research was supported by the NASA Upper Atmosphere Research Program under grant

NASA/NAG5-3980. Allocation of CPU time on the IBM SP supercomputer by the Supercomputing Institute for Digital Simulation and Advanced Computation at the University of Minnesota is also gratefully acknowledged. R.W.C. is pleased that this paper is included in this special issue of *J. Phys. Chem. A* honoring Charlie Parmenter, who has been a good and constant friend for these many years since our student days together at Rochester.

References and Notes

(1) Wallington, T. J.; Hurley, M. D.; Ball, J. C.; Kaiser, E. W. *Environ. Sci. Technol*. **1992**, *26*, 1318.

(2) Edney, E. O.; Driscoll, D. J. *Int. J. Chem. Kinet*. **1992**, *24*, 1067.

(3) Tuazon, E. C.; Atkinson, R. *J. Atmos. Chem*. **1993**, *16*, 301.

(4) Rattigan, O. V.; Rowley, D. M.; Wild, O.; Jones, R. L.; Cox, R. A. *J. Chem. Soc*. **1994**, *90*, 1819.

(5) Bednarik, G.; Breil, M.; Hoffman, A.; Kohlman, J. P.; Mörs, V.; Zellner, R. *Ber Bunsen-Ges. Phys. Chem*. **1996**, *100*, 528.

(6) Hasson, A. S.; Moore, C. M.; Smith, I. W. M. *Int. J. Chem. Kinet.* **1998**, *30*, 541.

(7) Wallington, T. J.; Hurley, M. D.; Fracheboud, J. M.; Orlando, J. J.; Tyndall, G. S.; Sehested, J.; Møgelberg, T. E.; Nielsen, O. J. *J. Phys. Chem*. **1996**, *100*, 18116.

(8) Maricq, M. M.; Szente, J. J. *J. Phys. Chem*. **1992**, *96*, 10862.

(9) Bhatnagar. A.; Carr, R. W. *Chem. Phys. Lett.* **1995**, *238*, 9.

(10) Schneider, W. F.; Wallington, T. J.; Barker, J. R.; Stahlberg, E. A. *Ber. Bunsen-Ges. Phys. Chem.* **1998**, *102*, 1850.

(11) Somnitz, H.; Zellner, R. *Phys. Chem. Chem. Phys.* **2001**, *3*, 2352.

(12) Wallington, T. J.; Kaiser, E. W. *Int. J. Chem. Kinet.* **1999**, *31*, 397.

(13) Møgelberg, T. E.; Sehested, J.; Wallington, T. J.; Nielsen, O. J. *Int. J. Chem. Kinet.* **1997**, *29*, 209.

(14) Moore, S. B.; Carr, R. W. *J. Phys. Chem*. **1990**, *94*, 1393.

(15) Wu, F.; Carr, R. W. *Int. J. Chem. Kinet.* **1991**, *23*, 701.

(16) Wu, F.; Carr, R. W. *J. Phys. Chem*. **2001**, *105*, 1423.

(17) Moore, S. B.; Carr, R. W. *Int. J. Mass Spectrosc. Ion Phys*. **1977**, *24*, 161.

(18) Olah, G. A.; Weber, T.; Farooq, O. *J. Fluorine Chem.* **1989**, *43*, 235.

(19) Curtiss, L. A.; Raghavachari, K.; Trucks, G. W.; Pople, J. A. *J. Chem. Phys.* **1991**, *94*, 7221.

(20) Curtiss, L. A.; Raghavachari, K.; Pople, J. A. *J. Chem. Phys.* **1993**, *98*, 1293.

(21) Foresman, J. B.; Frisch, Æ. *Exploring Chemistry with Electronic Structure Methods*, 2nd ed. Gaussian, Inc.: Pittsburgh, PA, 1996.

(22) Dixon, D. A.; Wiley, W. R. *Theoretical Calculations for the Reaction Pathways of Fluoroperoxy Radicals*; AFEAS Workshop, Washington, DC, May 21, 1997.

(23) Gilbert, R. G.; Smith, S. C.; Jordan, M. J. T. *UNIMOL Program Suite (Calculation of Fall-Off Curves for Unimolecular and Recombination Reactions)*, 1993; available from the authors: School of Chemistry, Sydney University, NSW 2006, Australia or by e-mail to gilbert_r@summer.chem.su.oz.au.

(24) Gilbert, R. G.; Smith, S. C. *Theory of Unimolecular and Recombination Reactions*; Blackwell Scientific Publications: Oxford, England, 1990.

(25) Lim, K. F.; Gilbert, R. G. *J. Chem. Phys.* **1986**, *84*, 6129.

(26) Reid, R. C.; Prausnitz, J. M.; Sherwood, T. K. *The Properties of Gases and Liquids*; McGraw-Hill: New York, 1977.

(27) Hirschfelder, J. O.; Curtiss, C. F.; Bird, R. B. *Molecular Theory of Gases and Liquids*; Wiley & Sons: New York, 1967.

(28) Troe, J. *Ber. Bunsen-Ges. Phys. Chem.* **1983**, *87*, 161.

(29) Atkinson, R.; Baulch, D. L.; Cox, R. A.; Hampson, R. F.; Kerr, J. A.; Troe, J. *J. Phys. Chem. Ref. Data* **1992**, *21*, 1125.

(30) Wu, F.; Carr, R. W. *J. Phys. Chem*. **1995**, *99*, 3128.

(31) Kaiser, E. W. *Int. J. Chem. Kinet.* **1993**, *25*, 667.

(32) Sehested, J.; Wallington, T. J. *Environ. Sci. Technol*. **1993**, *27*, 146.

(33) Sehested, J.; Mogelberg, T. E.; Fagerstrom, K.; Mahmoud, G.; Wallington, T. J. *Int. J. Chem. Kinet.* **1997**, *29*, 673.

(34) Louis, F.; Talhaoui, A.; Sawerysyn, J.-P.; Rayez, M.-T.; Rayez, J.-C. *J. Phys. Chem. A* **1997**, *101*, 8503.

(35) *Chemical Kinetics and Photochemical Data for Use in Stratospheric Modeling*; Evaluation No. 11, JPL Publication 97−4, 1997.

(36) Baer, S.; Hippler, H.; Rahn, R.; Seitzinger, N.; Troe, J. *J. Chem. Phys*. **1991**, *95*, 6463.

(37) Sehested, J.; Wallington, T. J. *Environ. Sci Technol.* **1993**, *27*, 146.

(38) Nielsen, O. J.; Sehested, J. *Chem. Phys. Lett.* **1993**, *213*, 433.

(39) Kaiser, E. W.; Wallington, T. J.; Hurley, M. D. *Int. J. Chem. Kinet.* **1995**, *27*, 205.

(40) Wu, F.; Carr, R. W. *J. Phys. Chem. A* **2002**, *106*, 5832.

(41) Atkinson, R. *Int. J. Chem. Kinet.* **1997**, *29*, 99.

(42) U.S. Standard Atmosphere. National Oceanic and Atmospheric Administration, 1976.

(43) Banks, P. M.; Kockarts, G. *Aeronomy*, part A, Academic Press: New York, 1973; pp 39−41.